Theoretical investigation of surface states and energetics of PtSi surfaces

Manish K. Niranjan*

Department of Physics, Indian Institute of Technology, Hyderabad, INDIA

ABSTRACT

Platinum silicide (PtSi) is highly promising material for applications in microelectronic devices. In this article, the surface electronic structure, surface energetics and workfunctions of stoichiometric and non-stoichiometric PtSi(010) surfaces are explored within the framework of first-principle density functional theory. The surface rumpling is found to be significant only for the top surface layer. The computed values of the rumpling parameter for the top three layers are ~11.0 %, ~0.9 % and ~1.9%. Further the interlayer relaxation is found to be largest for the top layer and decreases rapidly for inner layers. Localized surface states are obtained in the valence band at ~9.0 eV below the Fermi level. Under rich Pt and Si growth conditions, nonstoichiometric (010) terminations are found to have lowest surface energies, whereas stoichiometric termination has lowest surface energy (~1.74 J/m^2) under mixed conditions. The work function of stoichiometric (010) termination is computed to be 5.15 eV and differ as much as by ±0.5 eV for nonstoichiometric terminations.

(Keywords: Silicide; Surface electronic structure; Surface energies; Workfuntions; Ab-initio calculations)

I. INTRODUCTION

Metal silicides are highly promising materials for applications in silicon microelectronics [1,2,3,4,5,6,7,8,9,10,11,12]. Silicides with semiconducting properties have been found promising for applications in photovoltaics [13], optoelectronics [14], and as thermoelectric materials [15]. In addition to technological applications, silicides also exhibit diverse physical properties which make them attractive from solely scientific perspective. Silicides of iron, cobalt and manganese are now understood to be highly correlated electronic materials [16]. Furthermore, interesting phenomena such as quantum non-Fermi liquid behavior and critical phase transition have been observed in manganese silicide [17,18]. Metal silicides are used in complimentary metal-oxide-semiconductor (CMOS) devices to form Ohmic contacts, gate electrode and local interconnects due to their low contact resistance to Si, low resistivity, good thermal stability, and excellent process compatibility with standard Si technology. Over the years, titanium, cobalt, and nickel silicides have been used in CMOS device manufacturing. However, these silicides exhibit large Schottky barrier at silicon-silicide interface which results in relatively high contact resistance. In recent years, silicides of platinum have been found promising for application as contact materials in nanoscale CMOS devices due to their low Schottky barrier to *p*-type silicon and excellent thermal stability [2,3,19,20]. Besides application as contact materials in silicon based semiconductor devices, platinum silicides have also been successfully used in Schottky-barrier photodiodes (SBD) and detectors [1,2]. For instance, PtSi/*n*-Si junction based photodiode have found applications in multi-wavelength pyrometry and infrared (IR) imaging system. Schottky-barrier detectors are more advantageous over *p-n* junctions based detectors in that they are more robust in harsh radiation environment and are less prone to wear [21]. Furthermore, SBD are easy to integrate with Schottky-bipolar circuits which in turn provide superior radiation resistance.

During platinum silicidation reaction, two stable compositions, PtSi and Pt_2Si, are known to form in Pt-Si intermixed layers [20]. In the first reaction, Pt diffuses into Si resulting in the formation of intermediate compound Pt_2Si. Subsequently, in the second reaction, stable PtSi is formed as Si diffuses into Pt_2Si. Despite their technological importance, very few theoretical studies of platinum-silicides have been reported. In particular not much is known about their surface electronic structure and surface energetics. Recently, we reported a first-principles study of Schottky barrier height at Si/PtSi(010) interface [22]. In this article, we present a detailed study

of surface electronic structure and surface energies of stoichiometric and nonstoichiometric PtSi(010) surfaces. In addition, we also study the effect of surface defects on surface energies, workfunctions and electronic structure of PtSi(010) surfaces. The (010) termination is interesting in that it has low surface energy and promising for epitaxial growth of PtSi on Si substrate [5, 23, 24]. The knowledge of workfunction dependence on surface orientation and surface defects is important as it may have important implications for device applications [4, 6]. We also discuss the performance of LDA and GGA correlational functionals with regard to various computed parameters.

The rest of the paper is organized as follows. In Section II, computational methodology is presented. In section III, the crystal and electronic structure of PtSi are reviewed. The surface electronic structure of PtSi(010) surfaces are presented in section IV. Surface energies and workfunctions are discussed in section V. Concluding remarks are given in section VI.

II. COMPUTATIONAL METHDOLOGY

The calculations are performed using projected augmented wave (PAW) potentials within the framework of density functional theory as implemented in the VASP package [25]. The local-density approximation (LDA) and Pedew-Burke-Ernzerhof (PBE) form of generalized gradient approximation (GGA) are employed for exchange-correlation potentials [26,27]. The Kohn-Sham wavefunctions are expanded in plane wave basis set with a kinetic energy cutoff of 400 eV. The Brillouin zone of bulk PtSi is sampled using a 8x12x8 Monkhorst-Pack *k*-point mesh. Self-consistency in calculations is achieved until the total energies are converged to 10^{-6} eV/cell. The structures are relaxed until the largest force becomes less than 10^{-2} eV/Å. Surfaces are simulated using supercells with different number of PtSi(010) and vacuum layers. Symmetric slabs based on (1×1) surface cells are used with in-plane lateral lattice constants fixed to bulk values. Brillouin zone integrations are performed using 6x1x6 (or more) Monkhorst-Pack mesh and supercells are relaxed along growth direction until the forces on each atom is reduced to 0.01 eV/Å or less.

III. CRYSTAL AND ELECTRONIC STRUCTURE OF BULK PtSi

PtSi crystallizes in a primitive orthorhombic structure with *Pnma* space group symmetry (# 62 in the International X-Ray Tables) [28]. The unit cell consist four symmetry-equivalent Pt and four

symmetry equivalent Si atoms. The Pt and Si atoms are located on (010) plane at *b*/4 and 3*b*/4 positions. The computed and experimental lattice constants, fractional atomic coordinates, cohesive energy and heat of formation of PtSi are presented in Table 1. The fractional atomic coordinates of Pt and Si atoms are indicated as u_{Si}, u_{Pt}, v_{Si} and v_{Pt} for Si and Pt atoms. As can be seen from Table 1, the computed lattice constants and fractional atomic coordinates are in good agreement (~1-2%) with previously reported theoretical and experimental values [22, 28]. As expected, LDA and GGA computed values of lattice constants are underestimated and overestimated respectively as compared to experimental values. Further, the LDA and GGA computed cohesive energies are larger by ~19 % and ~1 % than experimental values. It may be noted that the LDA (GGA) are known to overestimate (underestimate) the value of cohesive energy of metals by ~20 % and 5% respectively [29]. Next, we summarize the electronic structure of bulk PtSi. The energy bands of bulk PtSi along high symmetry directions in the Brilliouin zone are shown in Fig. 1. The total and partial density of states (DOS) for PtSi are shown in Fig. 2. As can be seen, the states at the Fermi level in PtSi are derived primarily from 5*d* orbitals of Pt. The DOS in PtSi at the Fermi level are reduced significantly as compared to those in bulk Pt. This is indicative of poor metallic properties of PtSi as compared to that of pure bulk Pt. The reduction of DOS at Fermi energy in PtSi is expected due to Si mixing in pure Pt. As will be discussed in section V, low DOS at the Fermi energy in PtSi have implications for lower workfunctions of PtSi surfaces as compared to those for pure Pt surfaces. It is also clear from Fig. 1 and 2 that Pt 5*d* bands are relatively delocalized and contribute to entire valence band. The atomic structure of PtSi(010) surface is shown in Fig. 3. The valence charge density contours for this surface is shown in Fig. 4. As can be seen, the Pt and Si atoms form directional three center (Pt-Si-Pt) bonds in PtSi. Overall the bonding in PtSi can be described as mixed covalent-metallic.

IV. SURFACE ELECTRONIC STRUCTURE OF PtSi(010) SURFACES

Next, we study surface electronic structure of PtSi (010) surface. The PtSi(010) surface is stoichiometric (see Fig. 3) and has relatively low surface energy. Further PtSi(010) is suitable for epitaxial growth on Si(001) substrate due to small misfit strain. The stoichiometric PtSi(010)-(1x1) surface unit cell has two Pt and two Si atoms. After relaxation the PtSi(010) surface layers exhibit rumpling due to unequal forces acting on surface atoms (Pt and Si). The difference in

forces acting on surface atoms may be understood as arising due to difference in atomic polarizibility. The inward force is generally weaker on anions than on cations. The rumpling parameter δr_i is defined as:

$$\delta r_i = \left(r_i^{Pt} - r_i^{Si}\right)/ d_0 \qquad (1)$$

where $r_i^{Pt(Si)}$ are coordinates of Pt (Si) atoms in the ith layer along [010] direction and d_0 is bulk interlayer separation. Table 2 lists the computed rumpling parameter in PtSi(010) supercells composed of 13, 17, 21 and 25 layers. The LDA (GGA) computed values of the rumpling parameter for the top three layers $(\delta r_1, \delta r_2, \delta r_3)$ are obtained to be 11.0 % (10.5 %), 0.9 % (1.5 %) and 1.9 % (1.8 %) for supercell with 25 layers. This suggests that rumpling is significant only for the top surface layer. The magnitude of rumpling (~ 11% or ~ 0.2 Å) for the top PtSi(010) surface is comparable to that calculated for many binary semiconductor (GaAs) surfaces [30]. Table 2 also shows the results for percentage interlayer relaxation for unreconstructed stoichiometric PtSi(010) surface layers in supercells consisting 13, 15 , 21 and 25 layers. As can be seen, the LDA (GGA) computed interlayer spacing (Δd_{12}) between top two layers (in 25 layer supercell) exhibits contraction of 5.46% (5.51%). The interlayer spacing between second and third layers (Δd_{23}) is increased by 0.43% (0.80 %). It is evident that interlayer relaxation is largest for top surface layer and decreases rapidly for inner layers. In our calculations, only top interlayer spacing exhibits contractions, whereas spacing between other inner layers is increased. The contraction of first top layer interspacing (Δd_{12}) for PtSi(010) surface is expected and can be understood from Finnis-Heine model for surface relaxations [31]. The model predicts a small contraction for first interlayer spacing. In addition, it explains that the contraction is more pronounced for open surfaces than that for closed-packed. The top interlayer contraction occurs due to smoothening of electron charge density at the metal surface. As the metal surfaces are formed, the surface electrons rearrange themselves to reduce their kinetic energy thereby reducing the charge-density corrugations. This leads to surface electrons moving downward to the crystal. The downward movement of the electrons results in electrostatic attraction of top layer ions towards the crystal resulting in reduction of top interlayer spacing. The contraction of top interlayer spacing has been observed in several face-centered elemental metal surfaces [32]. The largest contraction is generally occurs for the (110) surface whereas the contractions at the (100) and particularly the (111) surfaces are small. Table 2 also indicates a small oscillatory

pattern in interlayer relaxations which may indicate Fridel oscillations in electron density driving the ions to relax [33]. Next, we study the electronic band structure of PtSi(010) surface. The bulk projected band structure of relaxed PtSi(010) surface supercell along high symmetry lines $\overline{\Gamma} - \overline{X} - \overline{U} - \overline{Z} - \overline{\Gamma} - \overline{U}$ is shown in Fig. 5. It can be seen that localized surface states occur deep in the PtSi valence band at ~ 9.0 eV below the Fermi level. Localized surface states can exist in the energy gap of the projected band structure of bulk material [34]. The charge density (planar averaged) along the slab axis projected on to these bands shown in Fig. 6a further indicate that these bands are localized within ~2 u.c from the top PtSi(010) surface layer. Furthermore, as evident from Figs. 6b-6c, the surface localized states are formed primarily by 5*d* and 3*s* orbitals of Pt and Si atoms located on top surface layer. Fig. 7 shows local density of states (LDOS) projected on atoms on first fours layers from top PtSi(010) surface. It is clear that surface electronic structure deviate from that of bulk only for first two layers. Further, the average width of DOS projected on 5*d* orbitals of Pt atoms on top surface layer is reduced (~0.4 eV) as compared to that for Pt atoms in bulk (see Fig. 7a). The reduction in the bandwidth is expected since the valence states are primarily comprised of localized 5d orbitals of Pt. The bandwidth is narrowed due to suppression of hopping integrals as the coordination numbers of surface atoms are reduced. The reduction in bandwidth of surface atoms is generally accompanied by shifting of the band towards or away from the Fermi energy. The Fig. 7a shows that Pt 5*d* band is shifted by ~0.25 eV towards the Fermi energy. The number of valence *d*-electrons per surface Pt atom is more than 5 and thus the rightward band shifting is expected from simple rectangular *d*-band model [35].

V. SURFACE ENERGETCS AND WORK FUNCTIONS

Next the surface energies and workfunctions of stoichiometric and nonstoichiometric PtSi(010) surfaces are calculated. The PtSi surfaces with Pt and Si defects are nonstoichiometric. The surface energies are known to vary with the orientation of the surface as they are related to number and strength of broken bonds at the surface. Thus, surface energies are lower for more closed-packed than those for open surfaces. Such variations in the free energy determine the shape of the crystal at equilibrium. Among all PtSi surface orientations, the stoichiometric (010) has the lowest surface energy as it is more closed packed compared to other orientations. However nonstoichiometric (010) and other surface orientations may have lower energies and

thus may be stabilized under appropriate experimental conditions. We calculate surface energies using Gibbs free energy formalism [36,37]. In this approach, the stable PtSi surface composition minimizes the surface free energy (γ) defined as

$$\gamma = \frac{1}{A}\left(G - \sum_i \mu_i N_i \right) \cong \tfrac{1}{2A}\left(E_{Slab} - N_{Si}\mu_{Si} - N_{Pt}\mu_{Pt} \right) \quad (2)$$

Here E_{slab} is the total energy of supercell used to simulate the surface. The factor of ½ is inserted since there are two equivalent surfaces per symmetric supercell. N_{Si} and N_{Pt} are the number of Si and Pt atoms respectively. μ_{Si} and μ_{Rh} are chemical potentials of Si and Pt atoms. The thermodynamic approach of stability of surfaces in terms of chemical potentials is suitable so long the surfaces are in equilibrium with their surroundings. Further, the experimental conditions can be simulated by considering appropriate values of chemical potentials. The chemical potentials also account for changes in total free energy when atoms are interchanged between the surface and the reservoir. The relative stability of surfaces can be predicted using Eq. (2) provided the surface is in equilibrium with bulk or any other reservoir. However, the present thermodynamic approach is not valid if reactions at the surface are not in equilibrium and/or governed by rate limiting kinetic factors. Since the bulk-surface system is in condensed phase, we ignore the dependence of chemical potentials on pressure and temperature. However, this dependence may not be ignored for gaseous phase systems [36]. The chemical potential of each atom in the system has an upper bound equal to chemical potential of the atom in elemental or bulk phase. In case of PtSi surface, pairs of Pt and Si atoms can be exchanged between surface and the bulk, provided PtSi surface is in equilibrium with bulk PtSi. Thus sum of chemical potentials of Pt and Si is equal to PtSi bulk energy per pair. Hence in equilibrium, the chemical potentials μ_{Si} and μ_{Rh} are related by the condition:

$$\mu_{Si} + \mu_{Pt} = \mu_{PtSi}^{(Bulk)} = \mu_{Pt}^{(Bulk)} + \mu_{Si}^{(Bulk)} - 2(\Delta H_f) \quad (3)$$

Where, $2(\Delta H_f)$ is the formation energy per formula unit of bulk PtSi (see Table 1). The surface energy can be expressed as:

$$E = \tfrac{1}{2}\left(E_{Slab} - N_{Si}\mu_{Pt}^{(Bulk)} - N_{Si}\mu_{Si}^{(Bulk)} + N_{Si}(2\Delta H_f) + \mu_{Pt}(N_{Si} - N_{Pt}) \right) \quad (4)$$

The surface is in equilibrium with its surrounding when the value of chemical potential lies within its upper and lower limits.

$$\mu_{Pt(Si)}^{(Bulk)} - 2\Delta H_f \leq \mu_{Pt(Si)} \leq \mu_{Pt(Si)}^{(Bulk)} \quad (5)$$

As listed in Table 3, the energy of PtSi(010) surface is calculated to be 1.74 J/m^2 (1.35 J/m^2) in LDA (GGA) approximation. As expected, the GGA computed surface energy is smaller by ~22% than that computed using LDA [35]. The LDA estimated surface energies can be expected to be more reliable than GGA estimated values due to favorable cancellation of errors in exchange and correlation energies [38]. Table 3 also shows PtSi(010) surface energies in supercells composed of 13, 17, 21 and 25 layers. As evident the surface energy changes by less than 1% as number of layers are increased. The computed PtSi surface energies may not be compared with experiments as no published experimental work exists on PtSi surface energies to best of our knowledge. However, PtSi(010) surface energy may be worth comparing with those obtained for pure Pt and Si surfaces. The calculated (LDA) energies of Pt(111) and Si(111) surface have been reported to be 2.22 J/m^2 and 1.36-1.74 J/m^2 respectively. These values are in reasonable agreement with reported experiment results [35,39]. The PtSi(010) surface energy can be expected to be lower than Pt surface energy due to Si alloying. For any material, the surface energy is generally a fraction of cohesive energy [35]. The surface and cohesive energies of many elemental metals have been found to satisfy following empirical relation.

$$E_{Surf} = \frac{\sqrt{C_{Bulk}} - \sqrt{C_{Surf}}}{\sqrt{C_{Bulk}}} E_{Coh} = \alpha E_{Coh} \quad (6)$$

Where E_{Surf} and E_{Coh} are surface and cohesive energies per atom. C_{Bulk} and C_{Surf} are coordination number of atoms in bulk and surface respectively. α is proportionality constant between surface energy and bulk cohesive energy. Using equa. (6), the value of α in PtSi comes out to be 0.18. The coordination number C_{Bulk} in bulk PtSi and C_{Surf} in PtSi(010) surface are 6 and 4 respectively. Using values from Table 1 and 3, α is calculated to be 0.14. This value is in reasonable agreement with one obtained using Eq. 6. Surface energies of stoichiometric PtSi (010) surface and those with vacancies and antisite defects as a function of Pt chemical potential are shown in Fig. 8. The upper limit of Pt chemical potential ($\mu_{Pt} = \mu_{Pt}^{(Bulk)} = 0$) in Fig. 8 indicate Pt rich environment in real experiments. The Pt chemical potential values higher than upper limit indicate the situation when bulk metallic Pt would start forming on the surface. The Si rich conditions corresponds to Pt chemical potential values near lower limit in Fig. 8. The bulk Si would form on surface if Pt chemical potential becomes smaller than its lower limit. Fig. 8 shows

that stoichiometric (010) surface has lowest surface energy (~1.74 J/m^2) for μ_{Pt} ranging from -1.2 to -0.4 eV. However under Pt rich conditions the energies of nonstoichiometric (010) surfaces with Si vacancies is lower than that of stoichiometric (010) surface. The energy is lowest for Pt terminated surface with vacancy of two Si atoms. Further, as expected, the surface energy of nonstoichiometric (010) surfaces with Si vacancies is lowest when growth conditions are Si rich.

Table 3 shows the workfunction of stoichiometric PtSi(010) surface calculated in LDA and GGA approximations and also for supercells of different sizes. The calculated workfunctions of nonstoichiometric (010) surfaces due to defects are tabulated in Table 4. Work function is calculated as difference between vacuum energy (E_{vac}) and Fermi energy (E_{Fermi}). In general, workfunction depends on orientation of metal surface and may vary from 0.1 to 1.0 eV. The workfunction arises due to redistribution of the charge density at the surface resulting in a dipole barrier [35]. As can be seen in Table 3, the work function of stoichiometric (010) surface is calculated to be 5.15 eV (4.96 eV) in LDA (GGA) approximations. However, it varies as much as by ±0.5 eV due to vacancy and antisite defects on surface (see Table 4). The computed work function comes out to be lowest (~ 4.63 eV) for (010) surface with two Pt atoms vacancies. Incidentally, the computed energy for this surface is also lowest under Si rich conditions (see Fig. 8). The workfunction is increased by 0.38 eV for (010) surface with two antisite Pt defects (Pt_{Si}). As can be seen in Fig.8, the thermodynamic energy of this surface is high under Si rich conditions. However under Pt rich conditions the energy is approximately equal to that of stoichiometric surface. The computed workfunction of PtSi(010) surface is lower than that of Pt surfaces (~5.70 eV). This is expected because of significant reduction of density of states in the vicinity of Fermi energy in bulk PtSi as compared to that in bulk Pt. The relatively small variation in workfunction indeed shows that PtSi should continue to be a promising material for applications in electronic devices.

VI. CONCLUSION

We have studied surface electronic structure, surface energetics and workfunctions of stoichiometric and non-stoichiometric PtSi(010) surfaces using first-principle density-functional theory. Only top surface layer is found to exhibit significant rumpling (~11%) and interlayer relaxation (~ -5.5 %). The localized surface states are found to exist at ~ -9.0 eV with respect to

Fermi energy (0.0 eV). The LDA (GGA) computed work function of stoichiometric PtSi (010) termination comes out to be 5.15 eV (4.96 eV). For nonstoichiometric (010) terminations the workfunction is found to vary as much as by ±0.5 eV as compared to workfunction of stoichiometric (010) termination. The surface energy of stoichiometric (010) termination is computed (LDA) to be ~1.74 J/m^2 which remains lowest under mixed conditions. However under Pt rich and Si rich growth conditions, the surface energies are found to be lower for nonstoichiometric (010) terminations. The obtained results are interesting from scientific and application point of view. We hope that the present study will stimulate further experimental and theoretical studies of PtSi surfaces.

ACKNOWLEDGEMENTS

This work was supported by the Department of Science and Technology (Grant No.: SR/FTP/PS-179/2011) and Supercomputing resources (PARAM Yuva-II) of Center for Development of Advanced Computing (CDAC), Government of India.

REFERENCES

* E-mail: manish@iith.ac.in; Tel: (91)9493595927; Fax: (91)040-23016032

1. S. P. Murarka, Silicides for VLSI applications, Academic Press (1983).
2 L. J. Chen, editor, Silicide Technology for integrated circuits, IEE, London (2004).
3. S. Zhang and M. Ostling, Crit. Rev. in Solid State and Mat. Sci., 28, 1 (2003).
4. S. M. Sze, Physics of Semiconductor Devices, 2nd ed. (Wiley, New York, 1981).
5. R. T. Tung, Mat. Sci. and Eng. R, 1, 1-138 (2001).
6. R. T. Tung, Appl. Phys. Rev., 1, 011304 (2014).
7. C. Detavernier, A. S. Özcan, J. Jordan-Sweet, E. A. Stach, J. Tersoff, F. M. Ross, and C. Lavoie, Nature, 426, 641 (2003).
8. Y. Lin, K. Lu, W. Wu, J. Bai, L. J. Chen, K. N. Tu, Y, Huang, Nano Letters, 8 (3), 913 (2008).
9. K. Lu, K. N. Tu, W. W. Wu, L. J. Chen, B. Yoo, N. V. Myung, Appl. Phys. Lett. 90, 253111 (2007).
10. B. Liu, Y. Wang, S. Dilts, T. S. Mayer, and S. E. Mohney, Nano Letters, 7 (3), 818 (2007).
11. M. K. Niranjan and U. V. Waghmare, J. App. Phys., 112, 093702 (2012).
12. M. K. NIranjan, V. S. Kumar, R. Karthikeyan, J. Phys. D: Appl. Phys., **47,** 285101 (2014)
13. S. Senthilarasu, R. Sathyamoorthy and S. Lalitha, Sol. Energy Mater. Sol. Cells, 82, 299–305 (2004).
14. J. Derrien, J. Chevrier, V. Lethanh and J. E. Mahan, Appl. Surf. Sci., 56–58, 382–393 (1992).
15. D. M. Rowe, CRC Handbook of Thermoelectrics, ch. 23–25, CRC Press, Boca Raton (1994).
16. P. S. Riseborough, Adv. Phys.,49, 257–320 (2000).
17. C. Pfleiderer, D. Reznik, L. Pintschovius, H. von Lohneysen, M. Garst and A. Rosch, Nature, 427, 227–231 (2004).
18. C. Pfleiderer, S. R. Julian and G. G. Lonzarich, Nature, 414, 427–430 (2001).
19. V. W. Chin, M. A. Green, and J. W. V. Storey, Solid-State Electron. 36, 1107 (1993).
20. G. Larrieu, E. Dubois,a) X. Wallart, and X. Baie, J. Katcki, J. Appl. Phys., 37, 921 (1966).
21. K. Solt, H. Melchior, U. Kroth, P. Kuschnerus, V. Persch, H. Rabus, M. Richter, and

G. Ulm, Appl. Phys. Lett., 69, 3662 (1996).
22. M. K. Niranjan, S. Zollner, L. Kleinman, A. A. Demkov, Phys. Rev. B, 73, 195332 (2006).
23. A. Wawro, S. Suto, A. Kasuya, Phys. Rev. B, 72, 205302 (2005).
24. R. T. Tung, J. M. Gibson, J. M. Poate, Phys. Rev. Lett., 50 429–32 (1983).
25. G. Kresse and J. Furthmuller, Phys. Rev. B, 54, 11169 (1996).
26. D. M. Ceperley and B. J. Alder, Phys. Rev. Lett., 45, 566 (1980).
27. J. P. Perdew, K. Burke, and M. Ernzerhoff, Phys. Rev. Lett., 77, 3865 (1996).
28. O. Beckstein, J. E. Klepeis, G. L. W. Hart, O. Pankratov, Phys. Rev. B, 63, 134112 (2001).
29. J. Paier, M. Marsman, K. Hummer, G. Kresse, I. D. Gerber, J. G. Angyan, J. Chem. Phys., 124, 154709 (2006).
30. F. Bottin, F. Finocchi, Phys. Rev. B, 76, 165427 (2007).
31. M. W. Finnis, V. Heine, J. Phys. F: Metal Phys., 4, 37 (1974).
32. F. Jona, J. Phys. C, 11, 4271 (1978).
33. J-h Cho, Ismail, Z. Zhang, E. W. Plummer, Phys. Rev. B, 59, 1677 (1999).
34. M. K. Niranjan, L. Kleinman, and A. A. Demkov, Phys. Rev. B, 77, 155316, (2008)
35. K. Wandel (ed.), Surface and Interface Science, Vol. 1, Willey-Vch (2012).
36. K. Reuter and M. Scheffler, Phys. Rev. B, 65, 035406, (2001).
37. M. K. Niranjan, L. Kleinman, and A. A. Demkov, Phys. Rev. B, 75, 085326, (2007)
38. V. K. Staroverov, G. E. Scuseria, J. Tao, J. P. Perdew, Phys. Rev. B, 69, 075102 (2004).
39. J. L. F. DaSilva, C. Stampfl, M. Scheffler, Surf. Sci., 600, 703 (2006).
40. E. J. Graeber, R. J. Baughman, and B. Morossin, Acta Crystallogr. 29, 1991 (1973).

Table 1: Computed (LDA and GGA) and experimental lattice constants (Å), fractional atomic coordinates, cohesive energy (E_{Coh}), heat of formation (ΔH_f) of bulk PtSi.

	a	b	c	u_{Pt}	v_{Pt}	u_{Si}	v_{Si}	E_{Coh} (eV/atom)	ΔH_f (eV/atom)
LDA	5.561	3.588	5.896	0.9983	0.1920	0.1783	0.5842	7.0	0.72
GGA	5.665	3.621	5.986	0.9951	0.1934	0.1781	0.5825	5.9	0.66
Exp.[a]	5.575	3.586	5.922	0.9956	0.1922	0.177	0.583	5.85	0.62

[a] Ref. [40]

Table 2: Computed percentage surface rumpling (δr_i) and interlayer relaxation (Δd_{ij}) in PtSi(010) supercells composed of 13, 17, 21 and 25 layers. Number starts from the top surface layer.

		13L	**17L**	**21L**	**25L**
δr_1	LDA	+11.2	+11.2	+11.2	+11.0
	GGA	+11.0	+10.8	+10.8	+10.5
δr_2	LDA	+0.9	+0.9	+0.8	+0.9
	GGA	+1.2	+1.5	+1.4	+1.5
δr_3	LDA	+1.7	+1.9	+2.0	+1.9
	GGA	+1.8	+1.8	+1.9	+1.8
δr_4	LDA	+0.9	+0.7	+0.7	+0.7
	GGA	+0.9	+0.9	+0.8	+0.9
Δd_{12}	LDA	-5.42	-5.33	-5.46	-5.47
	GGA	-5.72	-5.43	-5.59	-5.51
Δd_{23}	LDA	+0.53	+0.42	+0.42	+0.43
	GGA	+0.81	+0.77	+0.77	+0.81
Δd_{34}	LDA	+0.36	+0.27	+0.22	+0.21
	GGA	+0.48	+0.29	+0.27	+0.31
Δd_{45}	LDA	+0.20	+0.05	+0.02	+0.13
	GGA	+0.24	+0.13	+0.09	+0.08
Δd_{56}	LDA	+0.22	+0.15	+0.12	-0.01
	GGA	+0.31	+0.21	+0.21	+0.21
Δd_{67}	LDA	+0.31	+0.16	+0.10	+0.13
	GGA	+0.40	+0.22	+0.19	+0.16

Table 3: Surface energy (γ) and workfunction (φ) of stoichiometric PtSi(010) surface in supercells consisting 13, 17, 21 and 25 layers.

		13L	**17L**	**21L**	**25L**
γ (j/m^2)	LDA	1.74	1.73	1.73	1.71
	GGA	1.35	1.35	1.35	1.33
φ(eV)	LDA	5.15	5.14	5.15	5.15
	GGA	4.93	4.95	4.95	4.96

Table 4: Number of vacancy and antisite defects (n), areal density (ρ_A) of defects, and work function (φ) of nonstoichiometric PtSi(010) surfaces. Vacancy defect is indicated by letter "V". The subscript indicate the antisite defect. (See Fig. 8). The computations (LDA) are performed using PtSi(010) supercell consisting 17 layers.

		V_Si	**V_Pt**	**Si_{Pt}**	**Pt_{Si}**	**Si_{Pt}**	**Pt_{Si}**	**V_Si**	**V_Pt**	**V_PtSi**
n	0	1	1	1	1	2	2	2	2	2
ρ_A(10^{14}/cm^2)	0	3.05	3.05	3.05	3.05	6.10	6.01	6.01	6.01	6.01
φ(eV)	5.15	5.11	5.05	5.20	5.06	4.88	5.52	5.35	4.63	4.93

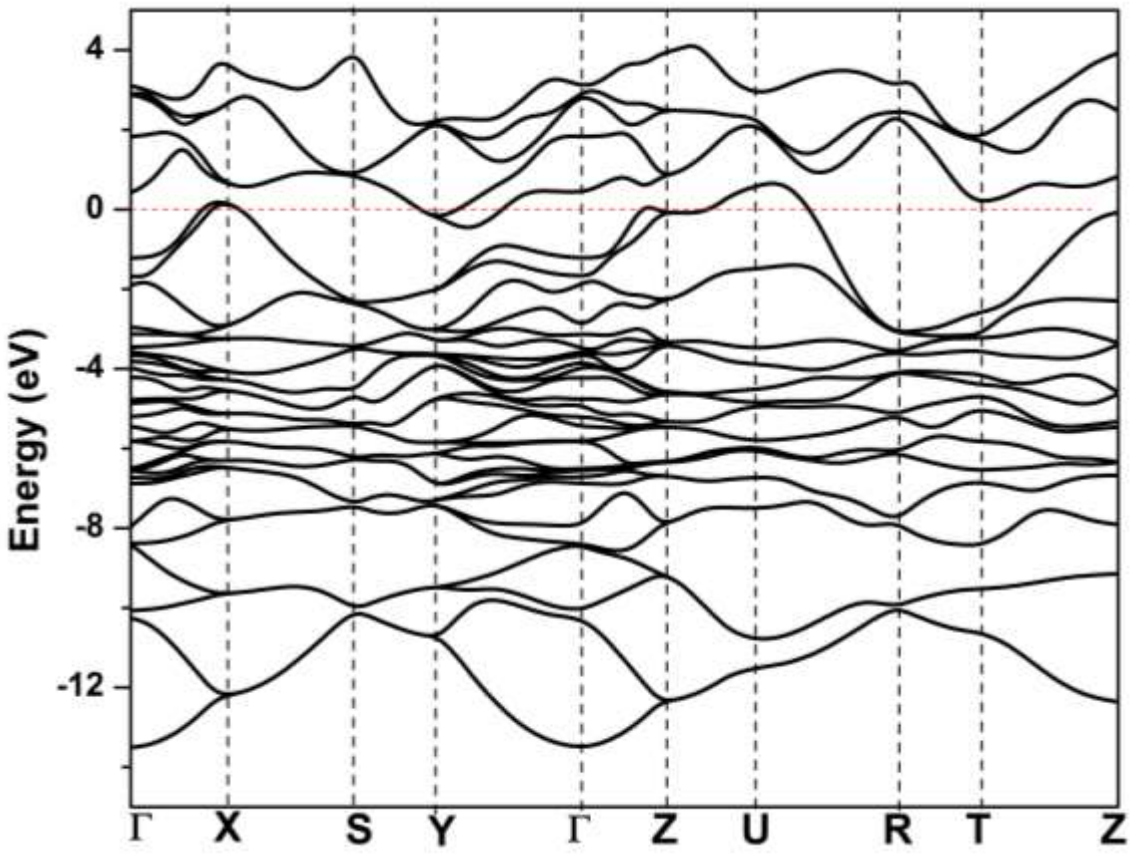

FIG. 1: Computed (LDA) energy band structure of bulk PtSi along high symmetry directions in the Brillouin zone of orthorhombic structure.

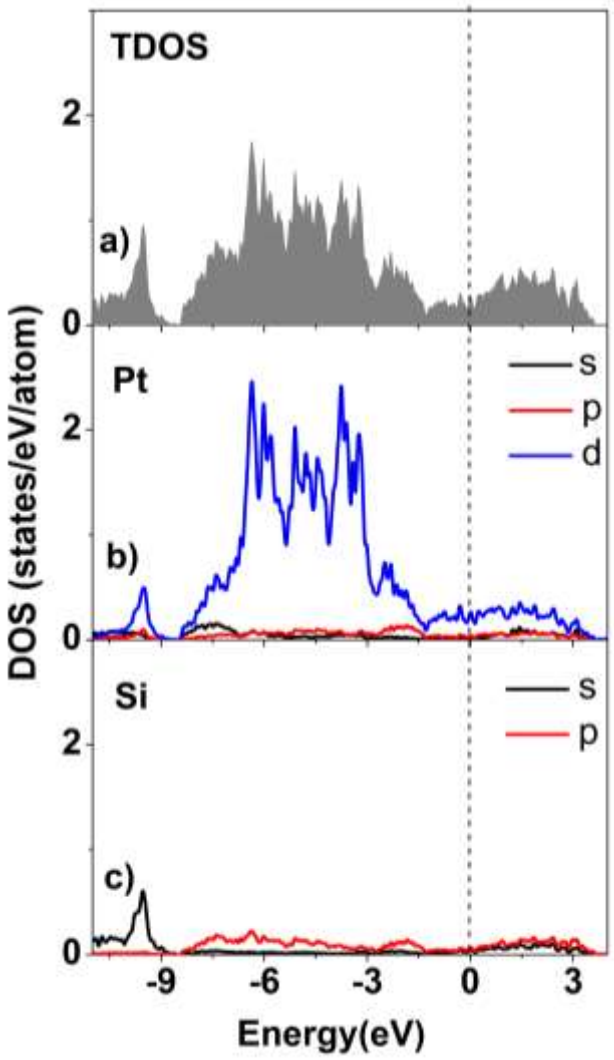

FIG. 2: (Color Online) Computed (LDA) **(a)** total density of states (DOS) in bulk PtSi. **(b)** Partial density of states in PtSi projected onto orbitals of Pt atoms. **(c)** Partial density of states in PtSi projected onto orbitals of Si atoms.

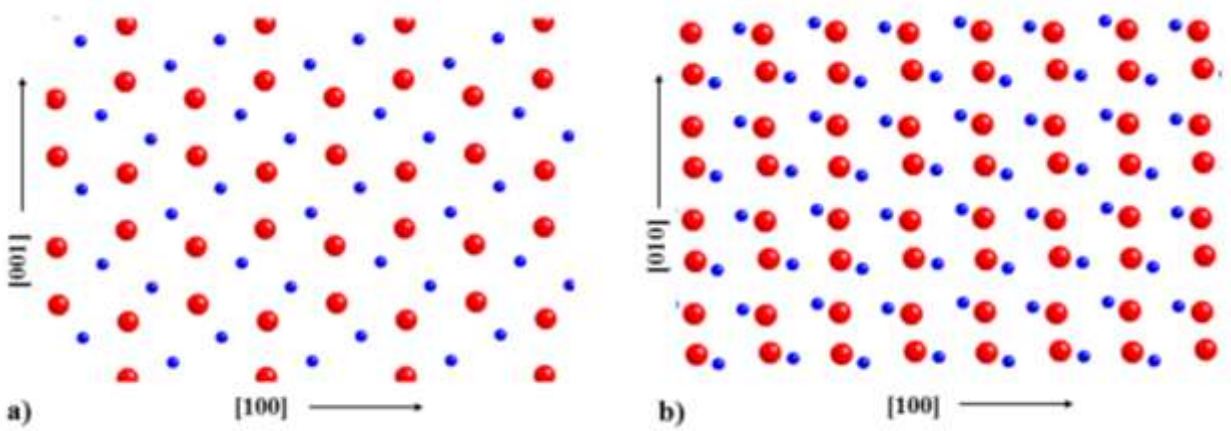

FIG. 3: (Color online) Atomic arrangement on (**a)** PtSi(010) surface (**b)** PtSi(001) surface. Big (red) and small (blue) balls are Pt and Si atoms respectively.

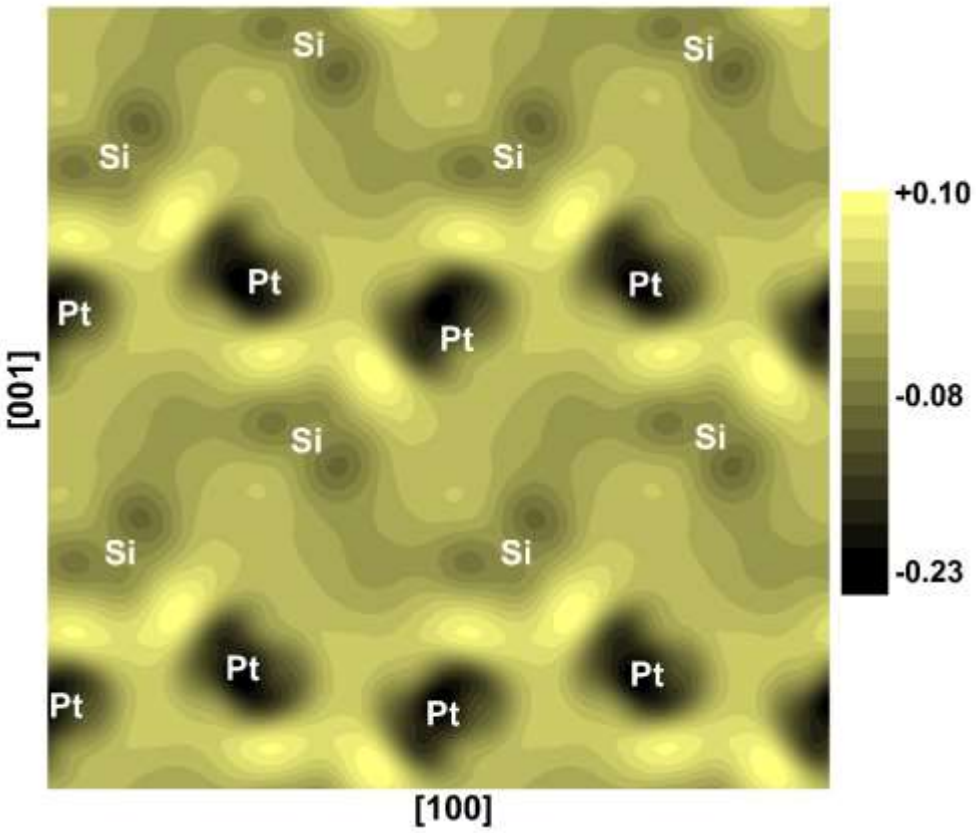

FIG. 4: (Color online) Computed (LDA) valence electron charge density contours in the (010) plane in PtSi unit cell.

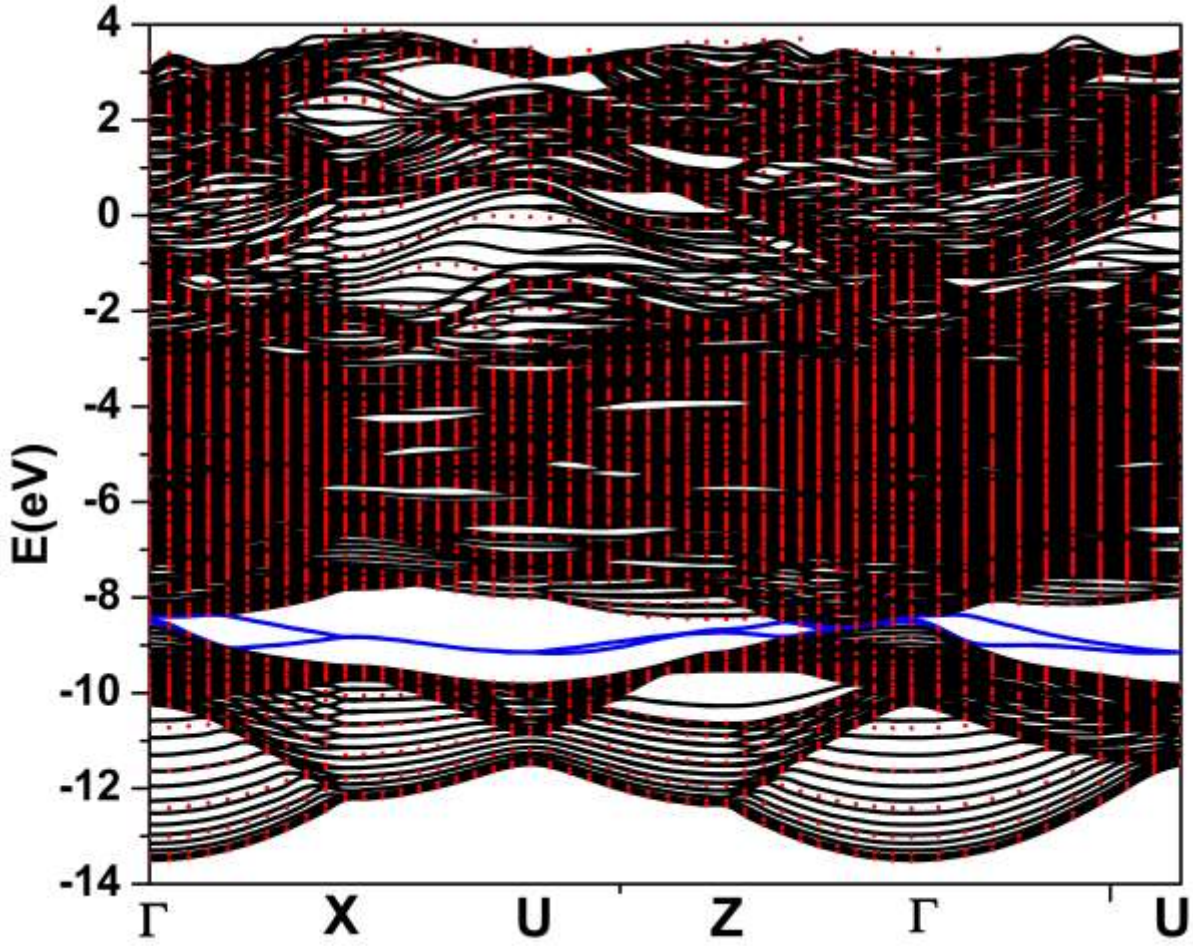

FIG. 5: (Color online) Computed (LDA) bulk projected band structure of relaxed PtSi(010) surface along $\overline{\Gamma} - \overline{X} - \overline{U} - \overline{Z} - \overline{\Gamma} - \overline{U}$ symmetry lines in the Brillouin zone. The projected bulk PtSi bands are indicated by red dots. Blue bands indicate localized surface states. The PtSi(010) supercell consists of 25 layers.

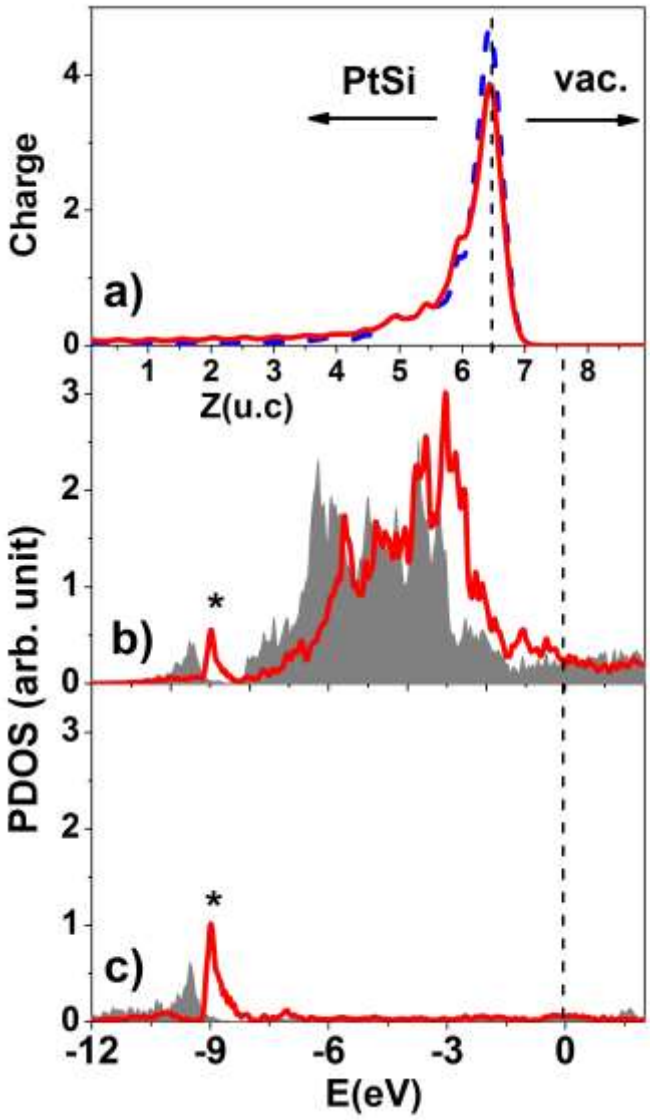

FIG. 6: (Color online) Computed (LDA) **(a)** planar averaged charge density along the PtSi(010) slab axis (in the units of lattice constant *b*) for the localized bands (~9 eV below Fermi energy) as shown in Fig. 5. The solid blue and dotted red lines indicate integration over all k-points and those along $\overline{\Gamma} - \overline{X} - \overline{U} - \overline{Z} - \overline{\Gamma} - \overline{U}$ symmetry line in the Brillouin zone. **(b)** Density of states projected on Pt atom on top surface layer (red) and in bulk (shaded). (**c)** Density of states projected on Si atom on top surface layer (red) and in bulk (shaded). Asterisk indicate localized states. The energy scale is with respect to Fermi energy at 0.0 eV. The PtSi(010) supercell consists of 25 layers.

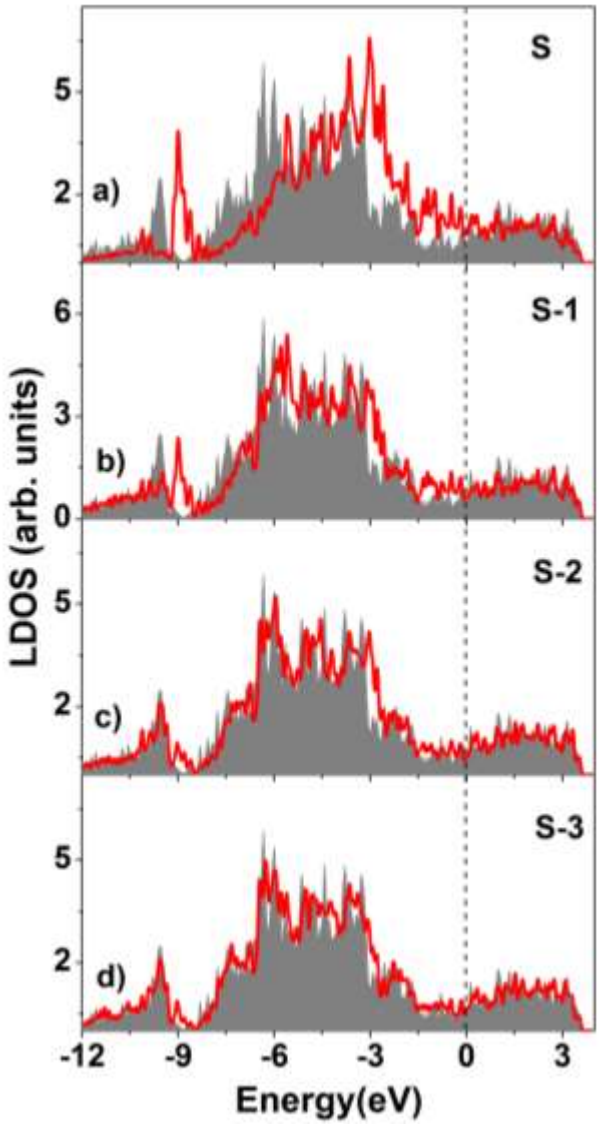

FIG. 7: (Color online) Computed (LDA) density of states projected on atoms in **a)** first layer (S) **b)** second layer (S-1) **c)** third layer (S-2) **d)** fourth layer (S-3) from top PtSi(010) surface. The DOS projected on atoms in bulk PtSi is indicated by shaded plot. The vertical line indicates the Fermi energy. The PtSi(010) supercell consists of 25 layers.

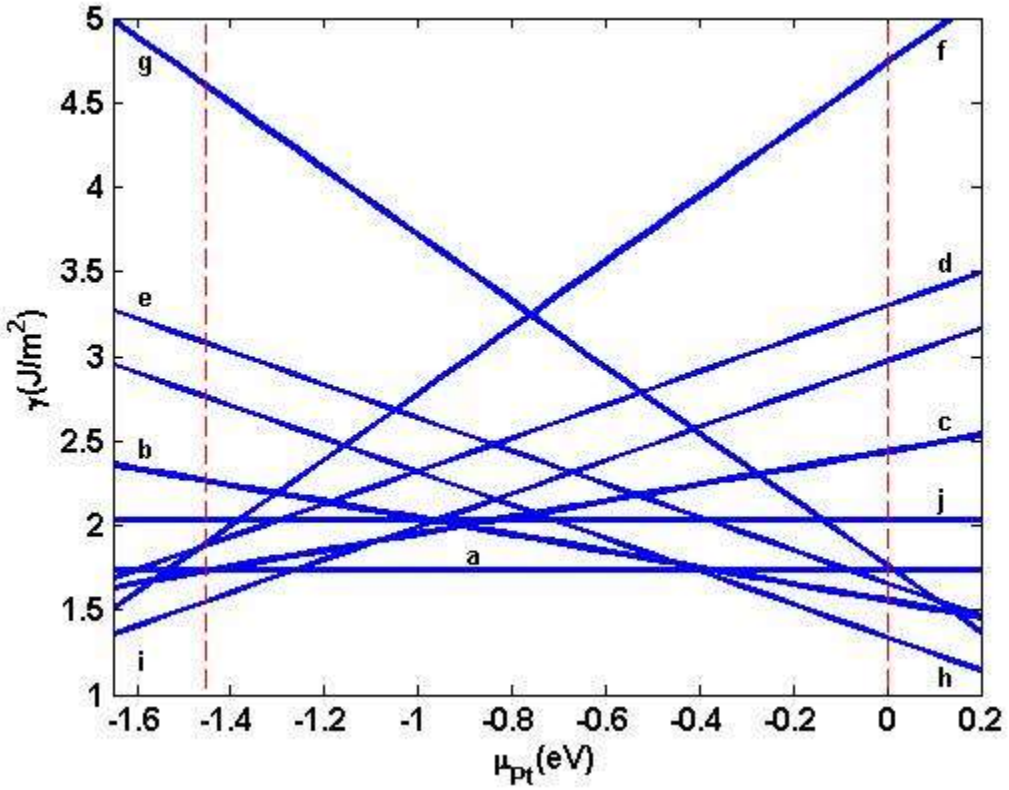

FIG. 8: Computed (LDA) surface energies of PtSi(010) surface (**a**) vacancy-free stoichiometric (0 V), (**b**) one Si atom vacancy (1 V_Si), (**c**) one Pt atom vacancy (1 V_Pt), (**d**) one antisite defect, Si at Pt site (1 Si_{Pt}), (**e**) one antisite defect, Pt at Si site (1 Pt_{Si}), (**f**) two antisite defects, Si at Pt sites (2 Si_{Pt}), (**g**) two antisite defects, Pt at Si sites (2 Pt_{Si}), (**h**) two Si atom vacancies (2 V_Si), (**i**) two Pt atom vacancies (2 V_Pt), (**j**) one Pt-Si pair vacancy (2 V_Pt-Si). The upper and lower limits of Pt chemical potential (μ_{Pt}) are indicated by dashed vertical lines. The PtSi(010) supercell consists of 17 layers.